Electronic energy levels of cinnabar (α-HgS)

E. Doni,* L. Resca,* S. Rodriguez, and W. M. Becker

Department of Physics, Purdue University, West Lafayette, Indiana 47907

(Received 9 April 1979)

We have calculated the electronic energy levels of trigonal mercury sulfide in the semiempirical tight-binding scheme. The atomic levels $3s, 3p$ of sulfur and $6s, 6p$ of mercury constitute the starting basis set. The computed two-center overlap integrals are subsequently scaled by a common multiplicative factor to reproduce the experimental optical gap. The effect of the atomic virtual level $4s$ of sulfur on the conduction bands is also taken into account. The calculated valence-band structure agrees well with the ultraviolet-photoelectron-spectroscopy (UPS) data. The complete band structure is consistent with the absorption measurements which indicate an indirect absorption edge immediately followed by the direct one (at the zone center). This picture can also explain the dependence of the absorption coefficient on the polarization of the exciting light in terms of the symmetry of the levels and the selection rules.

I. INTRODUCTION

The electronic band structure of cinnabar (α-HgS) is not yet known, even though the optical,[1-6] luminescence,[7] photoelectronic[8,9] and photoemission[10,11] properties of this material have been investigated to an appreciable extent on both natural and grown samples. Some experimental results[6,11] have been related in the past to the band structure which is available for meta-cinnabar (β-HgS),[12] the cubic modification of mercury sulfide which is unstable at room temperature. Due to the identity of the atomic constituents, it is reasonable to expect that some features of the electronic levels are indeed similar for the two phases. However, major differences in their electronic structures do occur, essentially because of their different crystal symmetries. Meta-cinnabar turns out to be a zero-gap semimetal, while cinnabar is an anisotropic semiconductor with strongly-temperature-dependent energy gap and highly dichroic character of the absorption coefficient. These properties make cinnabar a very interesting material, from both the fundamental and the technological point of view. In this work we report a semiempirical tight-binding (STB) calculation of the band structure of cinnabar.

II. BAND STRUCTURE OF CINNABAR

Cinnabar crystallizes in a trigonal lattice (space group D_3^4),[13] with a crystal structure similar to that of selenium and tellurium; mercury and sulfur atoms alternatively occur along a helical chain, with strong bonds linking each atom to the two adjacent ones of opposite species. Weaker forces act between different chains, as is indicated by the fact that cleavage planes always contain the chain axis. The lattice is described by the fundamental vectors

$$\vec{t}_1 = a\,[\tfrac{1}{2}, (\tfrac{3}{2})^{1/2}, 0], \ \vec{t}_2 = a\,[-\tfrac{1}{2}, (\tfrac{3}{2})^{1/2}, 0], \text{ and}$$

$\vec{t}_3 = c\,(0, 0, 1)$. The elementary cell contains three HgS molecules, the Hg atoms being in the positions

$$\vec{d}_1 = u\,(\vec{t}_1 - \vec{t}_2)\,, \quad \vec{d}_2 = u\vec{t}_2 + \tfrac{1}{3}\,\vec{t}_3\,,$$

and

$$\vec{d}_3 = -u\vec{t}_1 + \tfrac{2}{3}\,\vec{t}_3\,,$$

and the sulfur atoms being in the positions

$$\vec{d}_4 = v\vec{t}_1 + \tfrac{1}{6}\,\vec{t}_3\,, \quad \vec{d}_5 = -v\,(\vec{t}_1 - \vec{t}_2) + \tfrac{1}{2}\,\vec{t}_3$$

and

$$\vec{d}_6 = -v\vec{t}_2 + \tfrac{5}{6}\,\vec{t}_3\,.$$

The values of the parameters used in the calculation are[13] $a = 4.149$Å, $c = 9.495$ Å, $u = 0.28$, and $v = 0.485$. The minimum Hg-S distance is 2.36 Å, which is appreciably less than the sum of the covalent radii of sulfur and mercury.[14] This is an indication of the partially ionic nature of the main bond in the chain.

To obtain the crystal eigenvalues, we use a basis of Bloch functions derived from the atomic orbitals, $3s$, $3p$, and $4s$ of sulfur, and $6s$ and $6p$ of mercury. Therefore, we solve a secular determinant of order 27 at a generic point of the Brillouin zone (BZ). The atomic $5d$ levels of mercury are not included, even though their eigenvalue is close to that of the $3s$ atomic level of sulfur. The reason is that the d levels of mercury are highly concentrated around the nuclei and do not appreciably hybridize with other levels. On the other hand, the presence of the $3s$ orbitals of sulfur in the basis is necessary, in order to properly describe the directional bonds which form in the crystal because of the hybridizations with the $3p$ sulfur orbitals. For the same reason, the $6p$ virtual orbitals

of mercury must be included in the basis, even though they are not occupied in the ground state of the free atom. Furthermore, we include in an approximate way the virtual $4s$ level of sulfur, since it contributes to some important features of the lowest conduction bands. Similarly, in former tight-binding calculations for selenium,[15] the virtual $5s$ Se level could not have been omitted, and, as it has been recently pointed out, the anion virtual states are important for the lower conduction bands and for the crystal bondings of the ionic semiconductors.[16]

The Coulombic part of the crystal potential is written as a sum of atomic potentials. We compute these from the set of all the occupied orbitals of the free atoms which are given by Clementi et al.[17] The exchange part of the crystal potential is written in the $\rho^{1/3}$ approximation. It is then screened with the dielectric function as suggested by Robinson et al.,[18] which better includes correlation effects. To build our basis set, we use that atomic eigenfunctions $3s$ and $3p$ of sulfur and $6s$ of mercury as given by Clementi et al. in the Slater form.[17] No calculations of the virtual orbitals $6p$ of mercury and $4s$ of sulfur are available in the literature. As far as the Hg $6p$ levels are concerned, a satisfactory expression of the atomic radial eigenfunction can be obtained by assuming the Slater form with screening exponential factor identical to that of the $6s$ occupied orbital. This procedure is dictated by the standard Slater rules, since these s and p levels bear the same principal quantum number. The effect of the $4s$ virtual level of sulfur on the valence bands is going to be negligible, but we want to test the effect of a virtual state of the correct symmetry on the lowest conduction band. We can evaluate this continuously by assuming the $4s$ sulfur virtual orbital to be identical to the $3s$ sulfur orbital, and by treating the interactions parametrically: i.e., we scale all the integrals involving such a $4s$ orbital of sulfur by a common multiplicative factor p_1, which has then to be fitted to the experimental data.

We now have to determine the starting atomic eigenvalues. Due to the partially ionic nature of the main crystal bonds, intermediate values must be chosen between the eigenvalues of the free atoms and those of the free ions. Such a choice has to be consistent with the expression for the crystal field, which may vary continuously between a purely nonionic term and a purely ionic Madelung-type. An a priori evaluation of the ionicity can hardly give dependable results. According to photoemission experiments,[10,11] however, mercury $5d$ levels occur in cinnabar at 7.74 eV (weighted mean value of the spin-orbit split doublet) below the top of the valence band. Since we find, as a result of our calculation, that the top of valence bands in cinnabar always coincides with the eigenvalue of the sulfur $3p$ atomic orbital, we can evaluate the positions of sulfur atomic

eigenvalues relative to those of mercury in the crystal environment.

The absolute origin of the energy scale can be fixed by placing the top of the valence bands at -6 eV, which represents the experimental value of the work function (energy gap plus electronic affinity) in cinnabar.[11] In other words, the energy zero is set to coincide with the experimental vacuum level. The starting eigenvalues of the $6p$ and $4s$ virtual states of the free mercury and sulfur atoms, respectively, can be set to coincide with this energy zero. Virtual states of free atoms, as well as conduction bands in crystals, indeed relate to an extra electron added to the system. The electronic affinities of mercury and sulfur atoms for the $6p$ and $4s$ virtual levels are negligible if not zero. Note that excited states of the free atoms, which may have large negative energies because of the electron-hole interaction, may correspond to excitons in the crystal. The relationship can be very close if the crystal screening is small,[19] but this is not the case for cinnabar.

In the present calculation, we have taken into account all the interactions between couples of centers separated by less than 4.89 Å. All the relevant inter- and intrachain interactions are therefore considered. In addition to the factor p_1 which adjusts the $4s$ sulfur interactions, we introduce a second common multiplicative factor p_2 to scale all the computed overlap integrals. The factors p_1 and p_2 are the only free parameters of our model, and we vary them so as to produce a direct fundamental optical gap of about 2.2 eV. Furthermore, the values of the parameters are chosen to preserve the highest possible S-$4s$ interaction ($p_1 = 0.42$), and to retain the smallest possible overlaps ($p_2 = 0.25$). The reason is the following. In its standard formulation,[20] the STB method consists in computing all the relevant interaction and overlap integrals, and then slightly reducing them all in order to match some experimental features. It has been recently shown[21] that the multiplicative factor has actually to act only on the overlap integrals, with values close to zero (overlap reduced STB, ORSTB). The connection with the chemical pseudopotential approach[22] has been clearly shown. In such an approach, the secular equation does not contain the overlap integrals at all. Since the chemical pseudopotential only slightly differs from the atomic potential which is used in the standard TB theory, the difference accounts for retaining a small part of the overlaps in the ORSTB procedure. The reduction of the overlap integrals physically represents the contraction of the free-atom wave functions which takes place in the crystal.

We have tested the ORSTB procedure in the well-known case of selenium. We obtain the band structure for this material in almost perfect agreement with the results of Sandrock in the pseudopotential scheme.[23] This gives full confidence in the capability
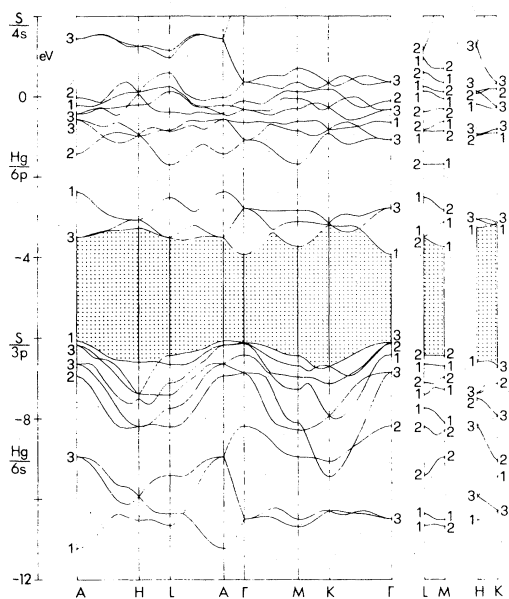
FIG. 1. Band structure of cinnabar.

of ORSTB to accurately provide the band structure of cinnabar. Selenium and cinnabar are indeed very similar crystals, which exhibit very close spectra and band structures, as we will discuss in Sec. III.

In Fig. 1, we exhibit the band structure of cinnabar as obtained with the ORSTB calculation. Crystal eigenvalues have been computed over more than 100 points along the lines of the BZ, which is shown in Fig. 2. At high-symmetry points, the eigenstates are labeled using the notations of Bradley and Cracknell[24] for the irreducible representations. The band-structure calculation has been double checked by using, in every symmetry point or line, symmetrized functions, which are obtained from the simple Bloch functions by means of an independent program.
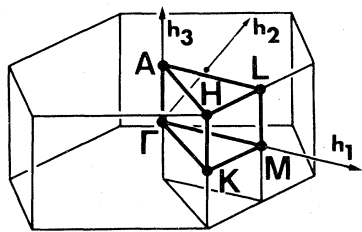

FIG. 2. Brillouin zone for cinnabar. Energy bands have been computed along the directions denoted by heavy lines.

III. DISCUSSION OF THE RESULTS AND COMPARISON WITH THE EXPERIMENTAL DATA

On the basis of the band structure of Fig. 1 and symmetry arguments,[25] we can interpret the following experimental features of the optical and photoemission spectra of cinnabar.

(i) The top of the valence band occurs at the point A of the BZ, and has symmetry A_1. The bottom of the conduction bands is instead at Γ, with symmetry Γ_1. Thus, cinnabar has an indirect absorption edge. In Fig. 3, we reproduce schematically the bands around the optical gap along the line A-Γ, and also indicate the selection rules. As we see from Fig. 3, the transition between A_1 and the lowest conduction state at A, i.e., A_3, is allowed only for light perpendicular to the axis of the chains (c axis) (at least as far as the single-group symmetry is concerned). This result agrees with the edge of the absorption spectrum of cinnabar obtained by Zallen,[1] who finds evidence for an indirect energy gap, with much larger transition probability for $\bar{E}\perp\bar{c}$ than for $\bar{E}\parallel\bar{c}$. For convenience, we show Zannen's[1] absorption spectrum in Fig. 4.

(ii) As we see in Figs. 1 and 3, the direct energy gap occurs at Γ, between the valence states Γ_3 and the conduction state Γ_1. The transition $\Gamma_3 \rightarrow \Gamma_1$ is also allowed only for light polarized perpendicular to the c axis. Spin-orbit interaction, however, relaxes this selection rule, and the transition becomes (weakly) allowed even for $\bar{E}\parallel\bar{c}$. In this respect, we therefore agree with Zallen's hypothesis[1] of a matrix-
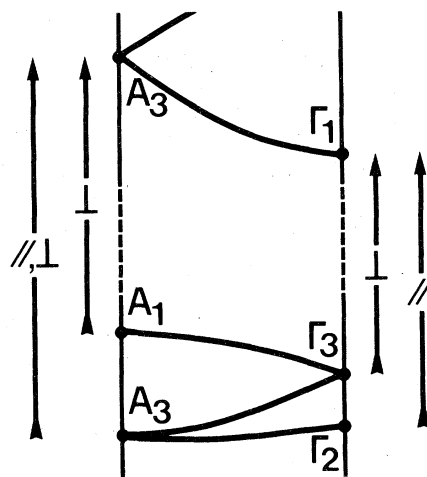
FIG. 3. Schematic representation of the three top valence bands and of the bottom conduction band of cinnabar along the A-Γ line. Transitions allowed for light parallel or perpendicular to the t_3 axis are indicated. Note that conduction and valence bands are not reproduced on the same scale.
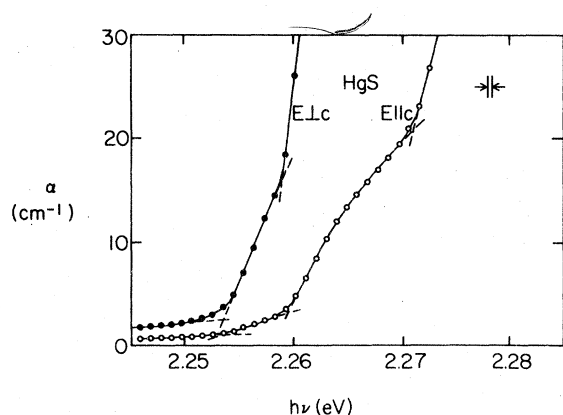
FIG. 4. Low-level edge absorption of HgS at 10°K, from Ref. 1.

element mechanism as responsible for the dichroism of HgS at the absorption edge. Furthermore, according to our calculation, the top valence band is quite flat along the line A-Γ, and it bends smoothly downward to merge at Γ in the two-dimensional representation Γ_3. The calculated difference between the levels A_1 and Γ_3 is about 0.05 eV. The order of these levels, and the order of magnitude of their difference, are preserved through any reasonable variation of the two parameters of our model. Therefore, this calculated difference compares well with the experimental value for the difference between direct and indirect gaps, as obtained by Zallen[1] from the absorption data. It should be noted, however, that the existence of the indirect gap is somewhat controversial in view of other experimental results.[1-9] It is not possible to definitely settle this question from a theoretical point of view, the energy difference between the indirect and the direct gap being too small. If we include for instance, the spin-orbit interaction in the ORSTB calculation, the Γ_3 level is split whereas the A_1 level is not. We expect Γ_3 to be split by nearly the atomic value for sulfur (0.09 eV), while A_1 can only be slightly shifted upward. Therefore, it is beyond the accuracy of the method to determine precisely where along the A-Γ line the minimum and the maximum of the conduction and valence bands, respectively, occur. The physical fact is, however, that the indirect and the direct gap are very close to one another, due to the flatness of the valence band and the shortness of the A-Γ line (in Fig. 1 the distances between consecutive points in the Brillouin zone are proportional to their true values). This results from the crystal structure which is very much elongated along the c axis.

(iii) We have found that the lowest conduction level Γ_1 is by far the most sensitive to the variation of the two adjustable parameters. In particular, it is very sensitive to the introduction of the $4s$ virtual or-

bital of sulfur in our basis set (p_1 value). Without the S $4s$ level ($p_1 = 0$), we obtain the bottom of the conduction bands at the point M, which produces an indirect absorption edge well below the direct gap; this does not seem to agree with the experimental evidence. The origin of this high sensitivity of the conduction level Γ_1 can be understood rather clearly if we consider the symmetrized combinations of Bloch sums at the Γ point, which are given in Table I. The highest Γ_1 level in the valence bands at Γ, and the lowest one in the conduction bands, correspond respectively mostly to the bonding and to the antibonding combinations of the $6s$ level of mercury with the $3p_x, 3p_y$ levels of sulfur. Due to the geometrical arrangement of mercury and sulfur atoms in the crystal, the antibonding combination tends to deprive the interior of the chain of charge, which is in turn spread outside the chain itself (along the external lobes of the p_x, p_y functions). Therefore, these crystal orbitals are the most sensitive to the interchain interactions, and to their variation with temperature. This accounts for the observed strong temperature dependence of the optical gap. [$\alpha = -9 \times 10^{-4}$ eV/K (Ref. 3), while for a typical semiconductor $\alpha \simeq -10^{-4}$ eV/K].

(iv) As far as the higher-energy region of the reflectivity spectrum is concerned, we note the close similarity between the cinnabar[5,6] and selenium[26,27] spectra up to about 4.5 eV.[28] This is due, according to our view, to the fact that the main contribution to the valence bands and to the three lowest conduction bands of cinnabar derives from the $3p$ orbitals of sulfur, just as it derives from the $4p$ orbitals in selenium. The reflectivity curves of selenium, however, decrease after 5 eV, and exhibit only minor structures in the higher-energy region. On the other hand, both α and β modifications of mercury sulfide show structures in the reflectivity spectra in the energy region between 5 and 7 eV. As a matter of fact, the imaginary part of the dielectric constant, which has been obtained up to now only for cubic HgS, shows in that very region the most relevant feature of the spectrum.[29] We associate these transitions with the $6p$ levels of mercury, which have no counterpart in the case of selenium. In Fig. 1, the set of bands in the range from -1.5 to 0.5 eV are mainly due to the presence of the Hg $6p$ orbitals. The large number of bands and their flatness over the BZ are responsible for the strong absorption which is revealed by the ϵ_2 curve of β-HgS between 5 and 7 eV.

(v) The ultraviolet photoemission spectrum (UPS), which we show in Fig. 5 for convenience from Ref. 11, exhibits two main regions of high density of valence states, in the range of 6 eV moving down from the top of the valence bands. The first region, with the main peak at 1.1 eV and a shoulder at 2.0 eV, is clearly produced by the six highest valence bands. Peaks in the density of states are expected in

TABLE I. Symmetrized combinations of Bloch sums at the point Γ. For instance, (Hg $6p_x$, 1) denotes the Bloch sum made up with the $6p_x$ atomic orbital of mercury centered on the site d_1. Similar notations hold for the other Bloch sums. Couples of partner functions are given for the two-dimensional representation Γ_3.

Γ_1: (Hg $6s$, 1) + (Hg $6s$, 2) + (Hg $6s$, 3)

(Hg $6p_x$, 1) $- \frac{1}{3}$(Hg $6p_x$, 2) $+ \frac{\sqrt{3}}{2}$(Hg $6p_y$, 2) $- \frac{1}{2}$(Hg $6p_x$, 3) $- \frac{\sqrt{3}}{2}$(Hg $6p_y$, 3)

(S $3s$, 4) + (S $3s$, 5) + (S $3s$, 6)

(S $3p_x$, 5) $- \frac{1}{2}$(S $3p_x$, 6) $+ \frac{\sqrt{3}}{2}$(S $3p_y$, 6) $- \frac{1}{2}$(S $3p_x$, 4) $- \frac{\sqrt{3}}{2}$(S $3p_y$, 4)

(S $4s$, 4) + (S $4s$, 5) + (S $4s$, 6)

Γ_2: (Hg $6p_y$, 1) $- \frac{\sqrt{3}}{2}$(Hg $6p_x$, 2) $- \frac{1}{2}$(Hg $6p_y$, 2) $+ \frac{\sqrt{3}}{2}$(Hg $6p_x$, 3) $- \frac{1}{2}$(Hg $6p_y$, 3)

(Hg $6p_z$, 1) + (Hg $6p_z$, 2) + (Hg $6p_z$, 3)

(S $3p_y$, 5) $- \frac{\sqrt{3}}{2}$(S $3p_x$, 6) $- \frac{1}{2}$(S $3p_y$, 6) $+ \frac{\sqrt{3}}{2}$(S $3p_x$, 4) $- \frac{1}{2}$(S $3p_y$, 4)

(S $3p_z$, 4) + (S $3p_z$, 5) + (S $3p_z$, 6)

Γ_3:

$\begin{cases} \text{(Hg } 6s, 1) - \frac{1}{2}\text{(Hg } 6s, 2) - \frac{1}{2}\text{(Hg } 6s, 3) \\ \frac{\sqrt{3}}{2}\text{(Hg } 6s, 2) - \frac{\sqrt{3}}{2}\text{(Hg } 6s, 3) \end{cases}$

$\begin{cases} \text{(Hg } 6p_x, 1) + \frac{1}{4}\text{(Hg } 6p_x, 2) - \frac{\sqrt{3}}{4}\text{(Hg } 6p_y, 2) + \frac{1}{4}\text{(Hg } 6p_x, 3) + \frac{\sqrt{3}}{4}\text{(Hg } 6p_y, 3) \\ -\frac{\sqrt{3}}{4}\text{(Hg } 6p_x, 2) + \frac{3}{4}\text{(Hg } 6p_y, 2) + \frac{\sqrt{3}}{4}\text{(Hg } 6p_x, 3) + \frac{3}{4}\text{(Hg } 6p_y, 3) \end{cases}$

$\begin{cases} \text{(Hg } 6p_x, 1) + \frac{5}{2}\text{(Hg } 6p_x, 2) + \frac{\sqrt{3}}{2}\text{(Hg } 6p_y, 2) + \frac{5}{2}\text{(Hg } 6p_x, 3) - \frac{\sqrt{3}}{2}\text{(Hg } 6p_y, 3) \\ 3\text{(Hg } 6p_y, 1) + \frac{\sqrt{3}}{2}\text{(Hg } 6p_x, 2) + \frac{3}{2}\text{(Hg } 6p_y, 2) - \frac{\sqrt{3}}{2}\text{(Hg } 6p_x, 3) + \frac{3}{2}\text{(Hg } 6p_y, 3) \end{cases}$

$\begin{cases} \frac{\sqrt{3}}{2}\text{(Hg } 6p_z, 2) - \frac{\sqrt{3}}{2}\text{(Hg } 6p_z, 3) \\ -\text{(Hg } 6p_z, 1) + \frac{1}{2}\text{(Hg } 6p_z, 2) + \frac{1}{2}\text{(Hg } 6p_z, 3) \end{cases}$

$\begin{cases} \text{(S } 3s, 5) - \frac{1}{2}\text{(S } 3s, 6) - \frac{1}{2}\text{(S } 3s, 4) \\ \frac{\sqrt{3}}{2}\text{(S } 3s, 6) - \frac{\sqrt{3}}{2}\text{(S } 3x, 4) \end{cases}$

$\begin{cases} \text{(S } 3p_x, 5) + \frac{1}{4}\text{(S } 3p_x, 6) - \frac{\sqrt{3}}{4}\text{(S } 3p_y, 6) + \frac{1}{4}\text{(S } 3p_x, 4) + \frac{\sqrt{3}}{4}\text{(S } 3p_y, 4) \\ -\frac{\sqrt{3}}{4}\text{(S } 3p_x, 6) + \frac{3}{4}\text{(S } 3p_y, 6) + \frac{\sqrt{3}}{4}\text{(S } 3p_x, 4) + \frac{3}{4}\text{(S } 3p_y, 4) \end{cases}$

$\begin{cases} \text{(S } 3p_x, 5) + \frac{5}{2}\text{(S } 3p_x, 6) + \frac{\sqrt{3}}{2}\text{(S } 3p_y, 6) + \frac{5}{2}\text{(S } 3p_x, 4) - \frac{\sqrt{3}}{2}\text{(S } 3p_y, 4) \\ 3\text{(S } 3p_y, 5) + \frac{\sqrt{3}}{2}\text{(S } 3p_x, 6) + \frac{3}{2}\text{(S } 3p_y, 6) - \frac{\sqrt{3}}{2}\text{(S } 3p_x, 4) + \frac{3}{2}\text{(S } 3p_y, 4) \end{cases}$

$\begin{cases} \frac{\sqrt{3}}{2}\text{(S } 3p_z, 6) - \frac{\sqrt{3}}{2}\text{(S } 3p_z, 4) \\ -\text{(S } 3p_z, 5) + \frac{1}{2}\text{(S } 3p_z, 6) + \frac{1}{2}\text{(S } 3p_z, 4) \end{cases}$

$\begin{cases} \text{(S } 4s, 5) - \frac{1}{2}\text{(S } 4s, 6) - \frac{1}{2}\text{(S } 4s, 4) \\ \frac{\sqrt{3}}{2}\text{(S } 4s, 6) - \frac{\sqrt{3}}{2}\text{(S } 4s, 4) \end{cases}$
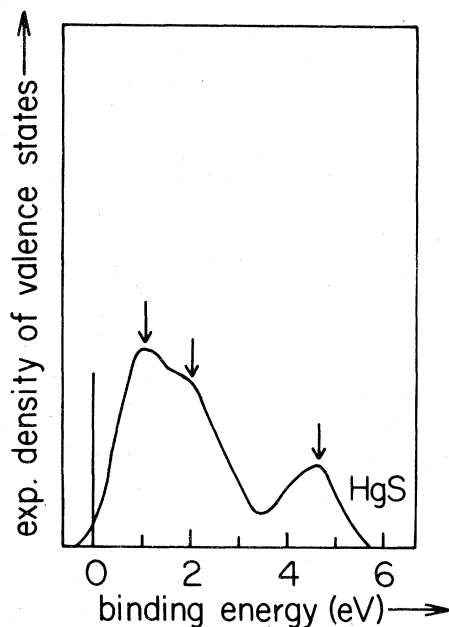
FIG. 5. Valence density of states for HgS determined from UPS data by Shevchik *et al.* (Ref. 11).

connection with saddle points in the $E(\vec{k})$ curve. These singularities occur mainly at the points H, L, K, and M of the boundary of the BZ (see Fig. 1). The UPS spectrum shows the second peak at the binding energy of 4.7 eV, with a slower decrease toward the low-binding energy side. The calculated bands fit these features well. Two nearly flat and isolated bands occur over a large part of the BZ in an energy range matching the experimental second peak (see Fig. 1). Furthermore, lower density-of-states structures are present at lower binding energies, before the second peak.

ACKNOWLEDGMENTS

*Permanent Address: Istituto di Fisica dell'Università, Pisa, Italy.

[1]R. Zallen, in *II-VI Semiconducting Compounds,* edited by D. G. Thomas (Benjamin, New York, 1967), p. 877.

[2]Ya. O. Dovgii, M. I. Brilinskii, and V. N. Korolishin, Sov. Phys. Semicond. 3, 87 (1969).

[3]M. Abkowitz, G. Pfister, and R. Zallen, J. Appl. Phys. 43, 2442 (1972).

[4]H. Langlois, thèse de 3° cycle (Université de Paris VI, 1973) (unpublished).

[5]M.-C. Lecocq-Mayer, thèse de 3° cycle (Université de Paris VI, 1975) (unpublished).

[6]V. I. Donetskikh and V. V. Sobolev, Opt. Spectrosc. (USSR) 42, 224 (1977).

[7]C. T. Simpson, W. T. Imaino, W. M. Becker, and S. P. Faile, Solid State Commun. 28, 39 (1978), and references quoted therein.

[8]G. G. Roberts, E. L. Lind, and E. A. Davis, J. Phys. Chem. Solids 30, 833 (1969).

[9]G. G. Roberts and R. Zallen, J. Phys. C 4, 1890 (1971).

[10]C. J. Vesely and D. W. Langer, Phys. Rev. B 4, 451 (1971).

[11]N. J. Shevchik, J. Tejeda, D. W. Langer, and M. Cardona, Phys. Status Solidi B 60, 345 (1973).

[12]F. Herman, R. L. Kortum, C. D. Kuglin, and J. L. Shay, in Ref. 1, p. 503; J. C. Phillips and J. A. Van Vechten, Phys. Rev. B 2, 2147 (1970).

[13]K. L. Aurivillius, Acta Chem. Scand. 4, 1413 (1950). For an accurate description of the cinnabar lattice, see also: R. Zallen, G. Lucovsky, W. Taylor, A. Pinczuk, and E. Burstein, Phys. Rev. B 1, 4058 (1970). Values of the lattice parameters slightly different from those used in the present paper are quoted by: M. A. Nusimovici and G. Gorre, Phys. Rev. B 8, 1648 (1973).

[14]L. Pauling, *The Nature of the Chemical Bond,* 3rd ed. (Cornell University, Ithaca, 1960), p. 246.

[15]D. J. Olechna and R. S. Knox, Phys. Rev. 140, A986 (1965).

[16]A. Baldereschi and K. Maschke in, *Proceedings of the 14th International Conference on the Physics of Semiconductors, Edinburgh, 1978,* edited by B. C. H. Wilson (Institute of Physics and Physical Society, London, 1979), p. 1167.

[17]E. Clementi and D. L. Raimondi, J. Chem. Phys. 38, 2686 (1963); E. Clementi, D. L. Raimondi, and W. P. Reinhardt, J. Chem. Phys. 47, 1300 (1967).

[18]J. E. Robinson, F. Bassani, R. S. Knox, and J. R. Schrieffer, Phys. Rev. Lett. 9, 215 (1962).

[19]L. Resca and R. Resta, Phys. Rev. B 19, 1683 (1979).

[20]F. Bassani and G. Pastori Parravicini, Nuovo Cimento B 50, 95 (1967).

[21]E. Doni, R. Girlanda, A. Balzarotti, V. Grasso, and M. Piacentini, Nuovo Cimento B (to be published).

[22]P. W. Anderson, Phys. Rev. 181, 25 (1969). See also: D. W. Bullett, J. Phys. C 8, 2695 (1975).

[23]R. Sandrock, Phys. Rev. 169, 642 (1968).

[24]C. J. Bradley and A. P. Cracknell, *The Mathematical Theory of Symmetry in Solids* (Clarendon, Oxford, 1972), p. 357.

[25]For symmetry notations, see Ref. 24. Selection rules are given for instance, by M. Hulin, J. Phys. Chem. Solids 27, 441 (1966).

[26]S. Tutihasi and I. Chen, Phys. Rev. 158, 623 (1967).

[27]E. Mohler, J. Stuki, and G. Zimmerer, Phys. Status Solidi 22, K49 (1967).

[28]Compare, for instance, Fig. III.3 of Ref. 5 with Fig. 1 of Ref. 7.

[29]Consider Fig. 2 given by H. D. Riccius and K. J. Siemens, *Proceedings of the Conference on the Physics of Semimetals and Narrow-Gap Semiconductors* (J. Phys. Chem. Solids 32, Suppl. 1, 1971), p. 493.